© 2017 Hefei Institutes of Physical Science, Chinese Academy of Sciences and IOP Publishing Printed in China and the UK

Plasma Sci. Technol. **19** (2017) 045502 (8pp) https://doi.org/10.1088/2058-6272/aa57f0

Fabrication and characterization of He-charged ODS-FeCrNi films deposited by a radio-frequency plasma magnetron sputtering technique

Liang SONG (宋亮)[1], Xianping WANG (王先平)[1], Le WANG (王乐)[1,2], Ying ZHANG (张营)[1,2], Wang LIU (刘旺)[1], Weibing JIANG (蒋卫斌)[1], Tao ZHANG (张涛)[1], Qianfeng FANG (方前锋)[1] and Changsong LIU (刘长松)[1]

[1] Key Laboratory of Materials Physics, Institute of Solid State Physics, Chinese Academy of Sciences, Hefei 230031, People's Republic of China
[2] University of Science and Technology of China, Hefei 230026, People's Republic of China

E-mail: xpwang@issp.ac.cn

Received 18 September 2016, revised 5 December 2016
Accepted for publication 5 December 2016
Published 9 March 2017

Abstract

He-charged oxide dispersion strengthened (ODS) FeCrNi films were prepared by a radio-frequency (RF) plasma magnetron sputtering method in a He and Ar mixed atmosphere at 150 °C. As a comparison, He-charged FeCrNi films were also fabricated at the same conditions through direct current (DC) plasma magnetron sputtering. The doping of He atoms and Y_2O_3 in the FeCrNi films was realized by the high backscattered rate of He ions and Y_2O_3/FeCrNi composite target sputtering method, respectively. Inductive coupled plasma (ICP) and x-ray photoelectron spectroscopy (XPS) analysis confirmed the existence of Y_2O_3 in FeCrNi films, and Y_2O_3 content hardly changed with sputtering He/Ar ratio. Cross-sectional scanning electron microscopy (SEM) shows that the FeCrNi films were composed of dense columnar nanocrystallines and the thickness of the films was obviously dependent on He/Ar ratio. Nanoindentation measurements revealed that the FeCrNi films fabricated through DC/RF plasma magnetron sputtering methods exhibited similar hardness values at each He/Ar ratio, while the dispersion of Y_2O_3 apparently increased the hardness of the films. Elastic recoil detection (ERD) showed that DC/RF magnetron sputtered FeCrNi films contained similar He amounts (~17 at.%). Compared with the minimal change of He level with depth in DC-sputtered films, the He amount decreases gradually in depth in the RF-sputtered films. The Y_2O_3-doped FeCrNi films were shown to exhibit much smaller amounts of He owing to the lower backscattering possibility of Y_2O_3 and the inhibition effect of nano-sized Y_2O_3 particles on the He element.

Keywords: radio-frequency plasma magnetron sputtering, He-charged FeCrNi-based film, nanoindentation hardness, elastic recoil detection, He implantation

(Some figures may appear in colour only in the online journal)

1. Introduction

The excellent properties in mechanical strength, creep and corrosion resistance mean that FeCrNi-based austenitic alloys are widely used as structural materials in nuclear systems [1, 2]. However, the high-energy neutron irradiation may cause radiation damage, which greatly changes the microstructure of structural materials and accordingly results in performance degradation, such as fatigue and creep [3–5]. Transmutation reactions induced by neutron irradiation

generally generate He atoms [6, 7], which tend to accumulate and be captured by defects in metals, precipitating into bubbles and leading to property deterioration of materials, in particular swelling and embrittlement [8, 9].

Therefore, reducing the degradation of the mechanical properties of structural materials in unclear environments is still a key challenge. It has been widely reported that oxide dispersion strengthened (ODS) steels show improved oxidation resistance and creep strength at high temperatures and high irradiation doses [10, 11], and such performance enhancement was ascribed to the stable nano-sized oxide particles and the interlocked structures between the matrix metal and reinforcing particle [12]. As an important hard ceramic oxide, Y_2O_3 oxide not only has a very high melting point ($\sim$2410 °C) but also exhibits strong structural and chemical stability under irradiation and corrosive environments. So in the design of high performance ODS alloys, nano-Y_2O_3 particles are generally chosen as an important dispersion phase to improve the high temperature strength, oxidation and irradiation resistance of base materials. Particularly in He embrittlement, the dispersion of nano-sized Y_2O_3 oxide particles can increase the number of He trapping and bubble nucleation sites for transmutation helium, which inhibit the agglomeration of helium atoms into coarse bubbles, and therefore minimizes the risk of helium embrittlement in structural materials for fusion reactor applications [13–15]. In this condition, systematic investigations into the preparation and He behavior of ODS steels are significant and meaningful.

Since first being reported by Mattox, who introduced He into gold films in 1971 [16], the magnetron sputtering method has been proved to be an effective way of introducing helium into metals. Recently, the magnetron sputtering method has been further developed into an easy and convenient method for introducing controllable amounts of He into metal films under a He and Ar mixed atmosphere by Shi, Liu and Jia [17–20]. During the film fabrication process, the ionized Ar sputters out the target atoms for depositing the film, while the ionized He atoms are mainly backscattered and implanted into the growing film because of the higher sputtering yield of Ar ions to metals than He atoms and the higher backscattering probability of He atoms than Ar atoms [21, 22]. Using the direct current (DC) plasma magnetron sputtering method, He atoms were also controllably introduced into nanocrystalline FeCrNi films and the amount of He element and its effects on the mechanical properties were carefully investigated in our previous work [23].

In order to fabricate ODS-FeCrNi films, insulating targets, which cannot conduct away positive ions that bombard the target, have to be sputtered, while for insulating targets in the DC sputtering process, the accumulation of positive charges increases the potential and then prohibits the process of sputtering. Radio-frequency (RF) plasma magnetron sputtering solves the problem by reversing the polarity of the power with a very high frequency ($\geqslant 10^{-7}$ s). The negative charges carried by the electrons would neutralize the positive charges on the target within 10^{-9} s, which ensures the continuity of the sputtering process. The oscillation of electrons

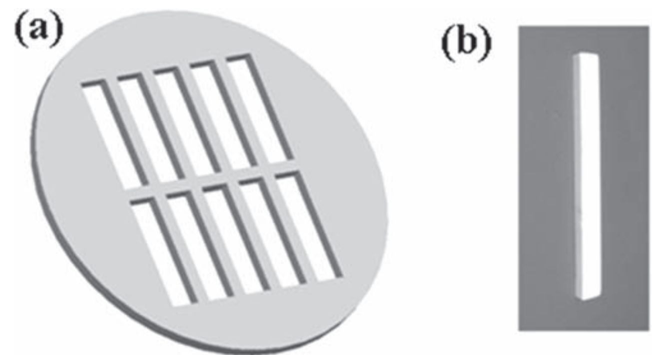

Figure 1. (a) 304 stainless target (b) Y_2O_3 ceramics for radio-frequency magnetron sputtering.

in the RF electric field enables them to absorb energy easily, which increases the ionization probability of Ar atoms and decreases the breakdown and discharge voltages of the sputtering process. Also, because of the low pressure needed to support RF magnetron sputtering, the atoms scattered from the targets are less likely to collide and lose energy, resulting in a higher bonding strength and compactness of the films.

In the present study, He-charged ODS-FeCrNi films were fabricated by the RF plasma magnetron sputtering method in a He and Ar mixed atmosphere. In the meantime, He-charge FeCrNi films were also prepared under the same conditions by DC and RF magnetron plasma sputtering for comparison. The commercial 304-stainless steel was used as the matrix target and Y_2O_3 ceramics were sintered for the doping of Y_2O_3 particles into the films. The morphology hardness and He content as well as depth of the He-charged FeCrNi-based films were characterized by scanning electron microscopy (SEM), nanoindentation measurements and elastic recoil detection (ERD), respectively.

2. Experiments

2.1. Preparation

Cylindrical 304-stainless steel discs (ϕ 60 mm $\times$ 3 mm) were cut as sputtering targets, and parts of them were further cut into the shape shown in figure 1(a), in which ten rectangular spaces with 19 mm length, 4.6 mm width and 2 mm thickness were arranged. Y_2O_3 powders of 40 nm diameter were ultrasonically vibrated for 1 h and dried in a ventilation oven. Then, the powders were divided into several parts of the same weight (1.5 g) and extruded into strips through a mold and a tableting machine. After being heated at 1400 °C for 5 h, the strips were sintered into Y_2O_3 ceramics (5 mm $\times$ 50 mm $\times$ 1.2 mm) with a relative density of 96%–97%, as shown in figure 1(b). After that, the Y_2O_3 dense strips were further polished into a suitable size and embedded into the targets, as shown in figure 1, to combine the composite targets used in RF magnetron sputtering. Silicon (Si) single crystal sheets with a (111) preferred orientation were used as the film substrates, and the experimental details were reported in elsewhere [23].

He-charged ODS-FeCrNi films were prepared on Si substrates through the RF magnetron plasma sputtering method in a He and Ar mixed atmosphere. The He/Ar ratio was adjusted by two separated mass flowing controllers. The substrate temperature was controlled at a constant value of 150 °C, which was considered as an optimum temperature for the fabrication of magnetron-sputtered films. Before depositing the FeCrNi-based films, the distance between the target and substrate was set to 60 mm and the sputtering pressure was evacuated by a turbo molecular pump to below 8.0×10^{-4} Pa. After adjusting the total pressure of He and Ar to about 1.5 Pa, the process of film preparation was carried out steadily for 4 h under a sputtering power of 50 W. The He/Ar ratios were modulated at 0, 1:1, 2:1 and 4:1, controlling the He partial pressure at 0, 50%, 67% and 80%, respectively, which introduce different concentrations of He into the ODS-FeCrNi films. To compare the effects of Y_2O_3 on film performance, He-charged FeCrNi films without Y_2O_3 were also prepared through DC/RF magnetron sputtering 304 stainless steel using the same parameters.

2.2. Characterization

After being dissolved and diluted into solutions with total element concentrations of $\leqslant$50 ppm, the elemental concentrations of Y_2O_3-added FeCrNi films were analyzed by atomic emission spectroscopy (AES) equipped with an inductive coupled plasma (ICP, iCAP 6000 SERIES) emission spectrometer, which can quantitatively determine the concentrations of Fe, Cr, Ni and Y in the films. To prepare the solutions, the films were precisely weighed and merged into the mixed acid of 1 ml HNO_3, 3 ml HCl and 6 ml deionized water in the beakers. After being sealed in the sample bags, the beakers were heated by an oven to 70 °C for 6 h until the films were completely dissolved. The solutions were diluted in flasks and further used in the analysis. X-ray photoelectron spectroscopy (XPS, Thermo ESCALAB 250) was conducted to characterize the existing forms of the Y element in the Y_2O_3-doped films. The light course was an Al K_α radiation ($h\nu = 1486.6$ eV) with a beam spot diameter of 500 μm, and the energy through the analyzer was fixed at 30 eV.

Surface and cross-sectional morphologies of the FeCrNi-based films were observed by field emission scanning electron microscopy (FESEM, Sirion 200 FEG) equipped with a secondary electron detector under the accelerating voltage of 10 keV. The nanoindentation hardness of the deposited films was measured by an Agilent Nano Indenter G200. The method of continuous stiffness measurement (CSM) makes it possible to obtain the hardness (H)-depth (h) profile with a single indent up to depth of about 2 μm, the maximum of which can be limited within the thickness of deposited films. Nine indents were performed on different areas of the film surfaces and the average nanoindentation hardness value deduced from the H–h profiles was used to represent the hardness of the films. During the process of nanoindentation, the resolution of displacement and load were about 0.02 nm and 50 nN, respectively. The backscattering possibilities and atom/ion sputtering yield of He and Ar were calculated by the SRIM code [24], and the corresponding simulation energy for He or Ar is 300 eV and the incident angle covered from 0° to 90°.

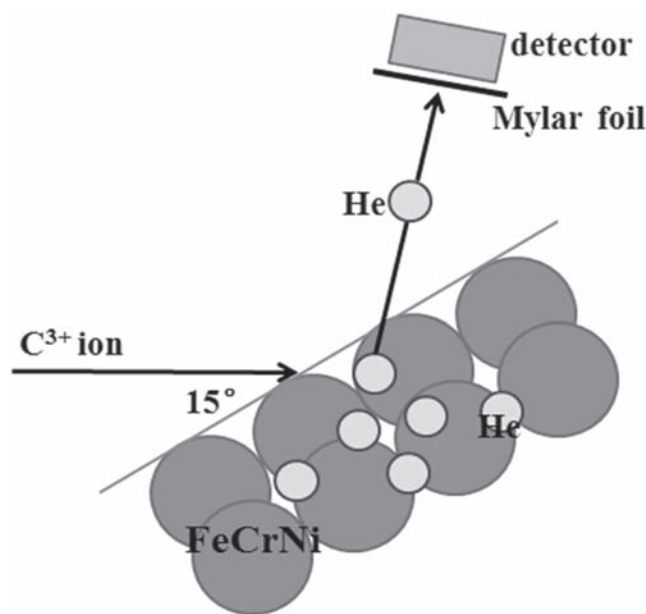

Figure 2. Schematic diagram of elastic recoil detection.

Table 1. Content of Y elements (at.%) in the films under different He/Ar ratios.

He/Ar ratio	Y at.%
0	4.27(8)
1:1	3.36(8)
2:1	3.40(0)
4:1	3.56(6)

To measure the He content in different film depths, elastic recoil detection (ERD) was conducted on an 8 MeV Tandem Accelerator at Institute of Modern Physics, Fudan University. As shown in figure 2, the ion beam was C^{3+} ions and the incident angle was 15°. A 10 μm-thick Mylar ($C_{10}H_8O_4$) foil was used as an absorbent sheet to retain irrelevant atoms and filter out the scattered He atoms to be recorded by the detector. All the ERD spectra were transferred to the helium concentration distribution by Alegria 1.2 codes [19, 25].

3. Results and discussion

3.1. Component analysis

Elemental concentrations of the Y_2O_3 added FeCrNi-based films prepared at 150 °C were quantitatively analyzed by AES-ICP, and the content of the Y element under different He/Ar ratios were listed in table 1. It clearly shows that the Y concentration changes only a little despite the change of sputtering atmosphere, which implies that the Y concentration

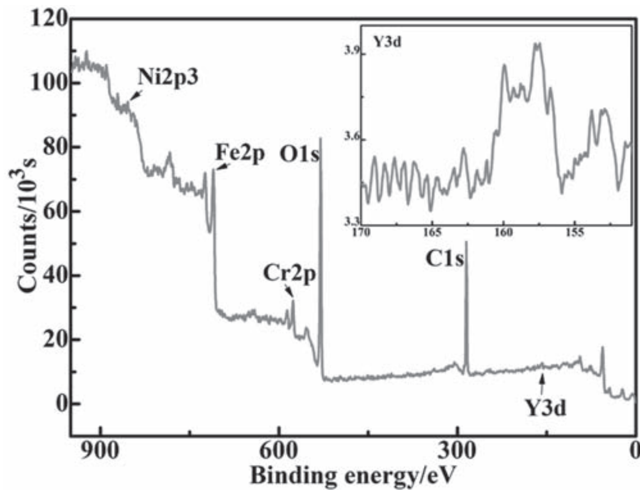

Figure 3. XPS pattern of the Y_2O_3-doped FeCrNi films fabricated on a Si substrate under He/Ar = 4:1 at 150 °C.

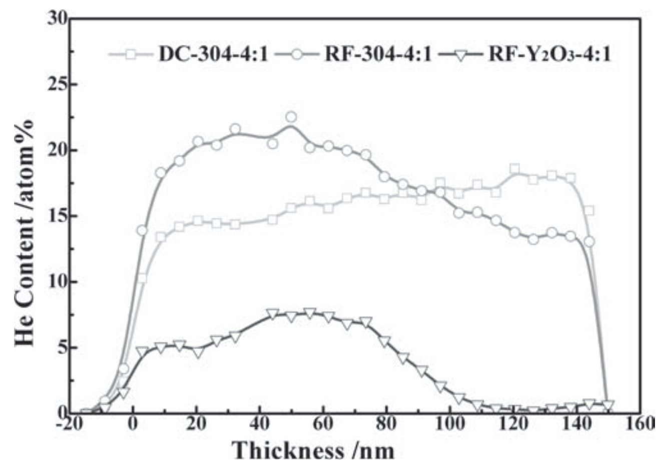

Figure 4. Helium content and distribution profiles in He-charged FeCrNi-based films fabricated through DC/RF magnetron sputtering under He/Ar = 4:1 at 150 °C.

in the ODS-FeCrNi films is almost independent of the He/Ar ratio.

Figure 3 shows the XPS pattern of the Y_2O_3-doped FeCrNi films fabricated through RF plasma magnetron sputtering under He/Ar = 4:1 at 150 °C. The binding energy of C1s was demarcated at 284.8 eV. After data correction, the peaks of Y3d were determined at 157.45–157.75 eV, which corresponds to the binding energy of Y3d5/2 electrons in Y_2O_3 molecules, indicating that the Y element exists as Y_2O_3 in the fabricated films.

3.2. He content and distribution

Figure 4 shows the He content versus depth for the He-charged FeCrNi-based film. It can be noted that the FeCrNi films fabricated by DC/RF magnetron sputtering a 304-stainless steel target contain a similar amount of helium (∼17 at.%), but the distribution of He in the films is slightly different. For the DC-sputtered film, the distribution of He atoms changes little with increasing depth, while for the RF sputtered sample, the He concentration decreases from ∼20 at.% around the surface to ∼14 at.% at the depth of 140 nm. However once a Y_2O_3/304 steel composite target is used, much less He (∼7 at.%) is introduced into Y_2O_3-doped FeCrNi films than that in the Y_2O_3 free FeCrNi films, as shown in figure 4. The reason may be related to the different backscattering rate of He on different materials. Table 2 gives the backscattering possibilities of He and Ar on 304 stainless steel and Y_2O_3 ceramics as calculated by SRIM. It is noted that for both 304 stainless steel and Y_2O_3 oxide, the backscattering possibility for He is much higher than that of Ar, leading to He atoms being easily implanted into the films in comparison with Ar atoms. Accordingly, the Ar ions are mainly to sputter out the target atoms owing to their heavy nuclei and much lower backscattering possibility.

Table 2. Backscattering possibilities of 304 stainless steel and Y_2O_3 ceramics on He and Ar.

	304 stainless steel	Y_2O_3 ceramics
He	0.338	0.264
Ar	0.047	0.062

On the other hand, the lower He level in the ODS-FeCrNi films detected by the ERD technique is also partially associated with the sink effects of nano-sized Y_2O_3 on He atoms. It was reported by Edmondson [13] and Lu [14] that nano-sized particles worked as trapping sites for He, which slowed their migration and nucleation centers of He bubbles, and therefore inhibited their further growth into large bubbles. Considering the capturing effects of nano-Y_2O_3 particles on He atoms and clusters in the ODS films, fewer He atoms would be bombarded out from the Y_2O_3-doped films and counted by the detector owing to the strong absorption of Y_2O_3 particles, resulting in a seemingly and relatively low atomic percentage of He in the Y_2O_3-doped films.

3.3. Microstructure characterization

Figure 5 gives the surface morphology of the He charged-FeCrNi-base films doped or undoped with Y_2O_3, which were fabricated through DC/RF plasma magnetron sputtering under He/Ar = 1:1 at 150 °C. As can be seen from this figure, the RF-sputtered films shown in figures 5(b) and (c) consist of smaller FeCrNi particles and have a smoother surface in comparison with the DC-sputtered film, and the addition of Y_2O_3 does not show obvious effects on film morphology. Further comparing the cross-sectional morphology of the He-charged FeCrNi films through different sputtering routes, it is found that the films all consist of dense columnar nanocrystals, as shown in figure 6, and the thickness of the DC-sputtered, RF-sputtered and RF-sputtered Y_2O_3-doped FeCrNi films are 4.7 μm, 2.2 μm, and 1.6 μm, respectively. It is noted that the columnar crystals in the film fabricated through RF magnetron sputtering are seemly finer and more uniform than those in the FeCrNi films fabricated through DC magnetron sputtering, which is consistant with the results of surface morphology.

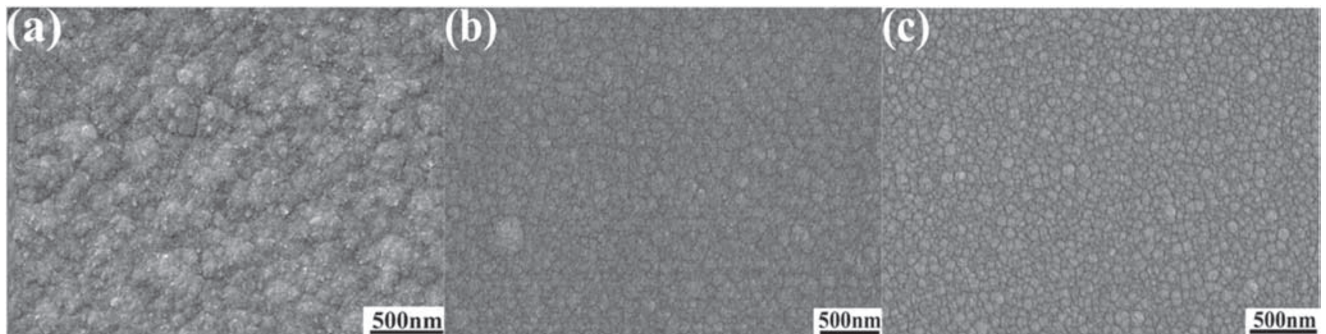

Figure 5. Surface morphology of FeCrNi-base films doped/undoped with Y_2O_3 fabricated on a Si substrate through DC/RF magnetron sputtering under He/Ar = 1:1 at 150 °C: (a) DC-sputtered FeCrNi films, (b) RF-sputtered FeCrNi films, (c) RF-sputtered Y_2O_3-doped FeCrNi films.

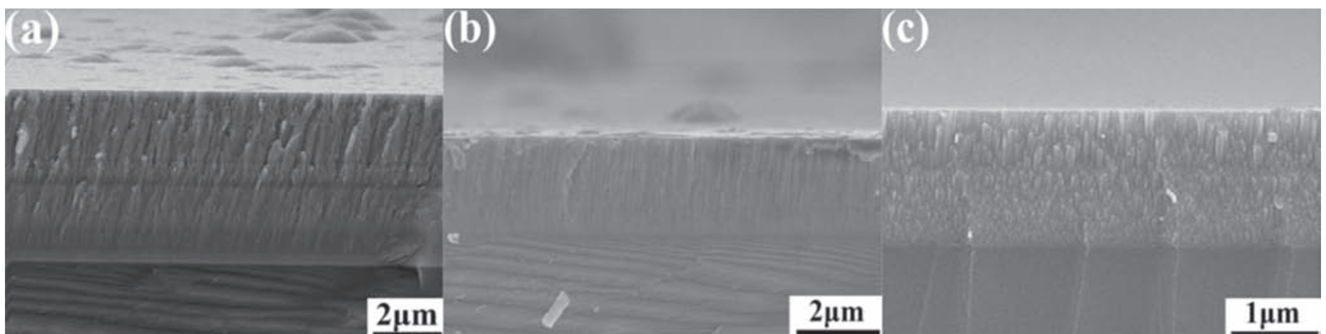

Figure 6. Cross-sectional morphology of the He-charged FeCrNi-based films fabricated on a Si substrate under He/Ar = 1:1 at 150 °C: (a) DC-sputtered FeCrNi films, (b) RF-sputtered FeCrNi films, (c) RF-sputtered Y_2O_3-doped FeCrNi films.

To evaluate the effects of partial He pressure on film surfaces morphology, different He/Ar ratios were used during the process of fabricating Y_2O_3-doped films under the same sputtering temperature of 150 °C, as shown in figure 7. Although all the prepared films are found to consist of small particles of a similar size, the particle-aggregated clusters become smaller and the cluster-formed surface becomes smoother as the He/Ar ratio increases from 0 to 2:1. Further increasing He/Ar ratio to 4:1, irregular embossments appear randomly on the smooth surface.

The cross-sectional morphologies of Y_2O_3-containing FeCrNi films fabricated through RF magnetron sputtering under different He/Ar ratios are shown in figure 8, and the corresponding thickness under different He/Ar ratios is 1.5 μm, 1.3 μm, 1.0 μm and 0.9 μm respectively with increasing He/Ar ratio. The results indicate that as the He/Ar ratio increases in the mixed atmosphere, the He partial pressure increases and the sputtering rate of the target accordingly decreases, leading to a reduction in the thickness of the deposited films. Further comparing the Y_2O_3-free and Y_2O_3-containing FeCrNi films, the thickness in the Y_2O_3-added FeCrNi films is smaller than that in the Y_2O_3-free films under the same sputtering parameters, and this can be explained in terms of the different sputtering yields of He and Ar on 304 stainless steel and Y_2O_3 ceramics simulated by the SRIM program, as shown in table 3. Because of the smaller sputtering yield of He and Ar on Y_2O_3 ceramics than on 304 stainless steel, the films fabricated through sputtering Y_2O_3/304 stainless steel composite targets are thinner than that of the Y_2O_3 free films.

3.4. Nanoindentation

In order to investigate the influence of the He/Ar ratio and Y_2O_3 dispersion on the mechanical properties, the nanoindentation technique was used to evaluate the hardness of the fabricated FeCrNi-based films. Three typical indentation-depth curves of the Y_2O_3-doped FeCrNi films prepared under He/Ar = 4:1 are shown in figure 9. Due to the effects of surface roughness and limitations of the CSM technique [26, 27], the values of hardness fluctuate in the indentation-depth range less than 200 nm. However, no significant difference is observed in the profiles of each single indent when the indentation is deeper than 200 nm. Thus, the nano-hardness of the ODS films deposited under each condition was consequently obtained through averaging the values of hardness-depth profiles located around 500 nm–1000 nm.

Figure 10 presents the nanoindentation hardness of FeCrNi-based films versus He/Ar ratio under different conditions, which are DC sputtered 304 stainless steel, RF sputtered 304 stainless steel and the Y_2O_3/304 composite target, respectively. It is noted that the undoped FeCrNi films fabricated by DC/RF magnetron sputtering methods exhibit close nanoindentation hardness under the same sputtering atmosphere, which implies that the mode of magnetron sputtering does not greatly affect the mechanical properties of the films. However once He atoms were implanted into the

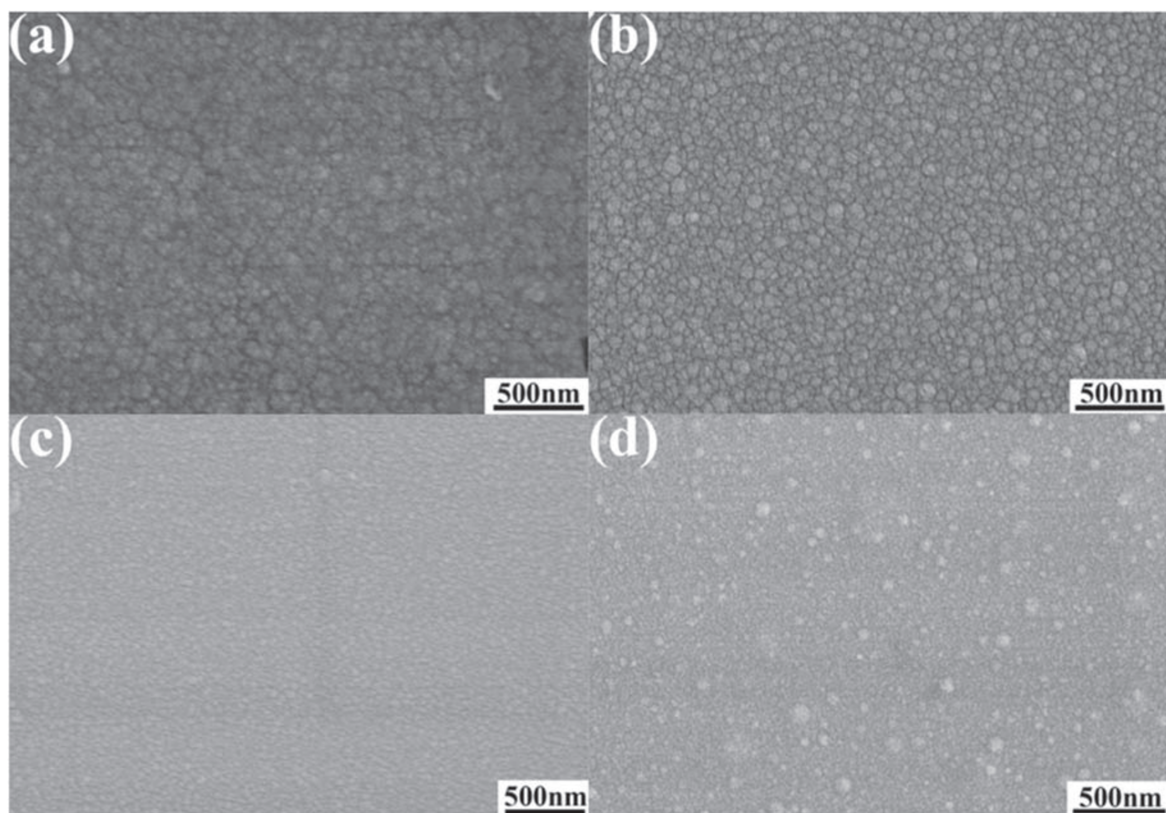

Figure 7. Surface morphologies of the films fabricated on Si substrates under different He/Ar ratios at 150 °C , He/Ar = (a) 0; (b) 1:1; (c) 2:1; (d) 4:1.

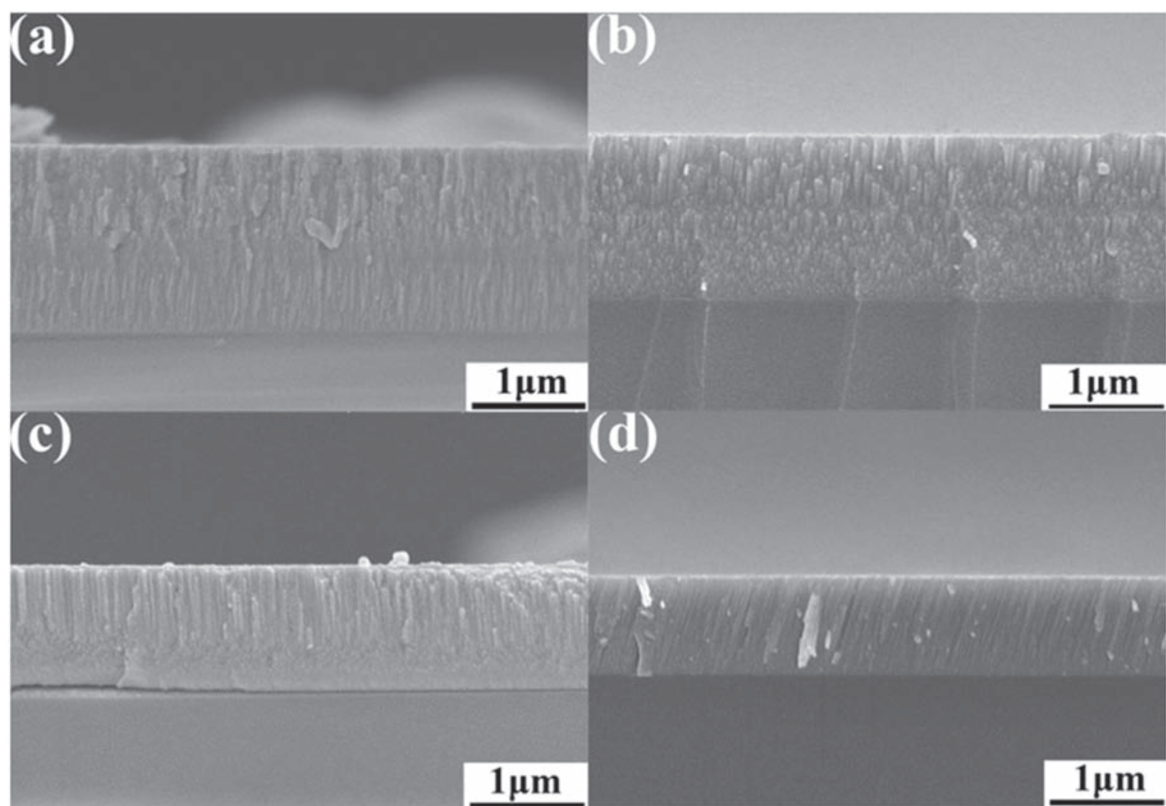

Figure 8. Cross-sectional morphology of Y_2O_3-doped FeCrNi films fabricated on a Si substrate through RF magnetron sputtering under different He/Ar ratios at 150 °C, He/Ar = (a) 0; (b) 1:1; (c) 2:1; (d) 4:1.

Table 3. Atoms/ion sputtering yield of He and Ar on 304 stainless steel and Y_2O_3 ceramics.

	304 stainless steel	Y_2O_3
Ar	1.310	0.221
He	0.210	0.042

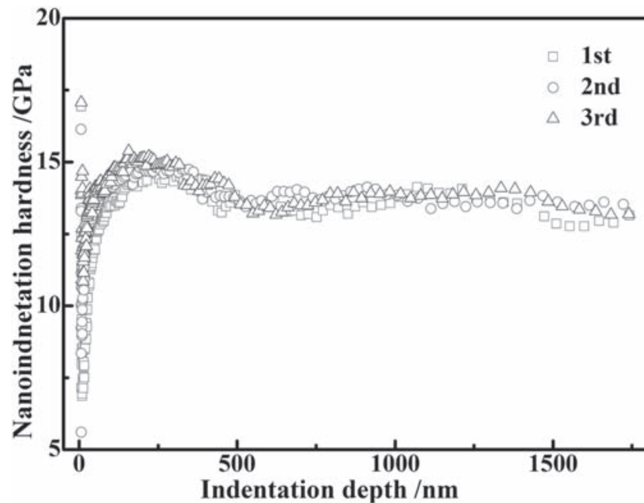

Figure 9. Representative indentation-depth profiles of the Y_2O_3-doped FeCrNi film fabricated under He/Ar = 4:1 at 150 °C.

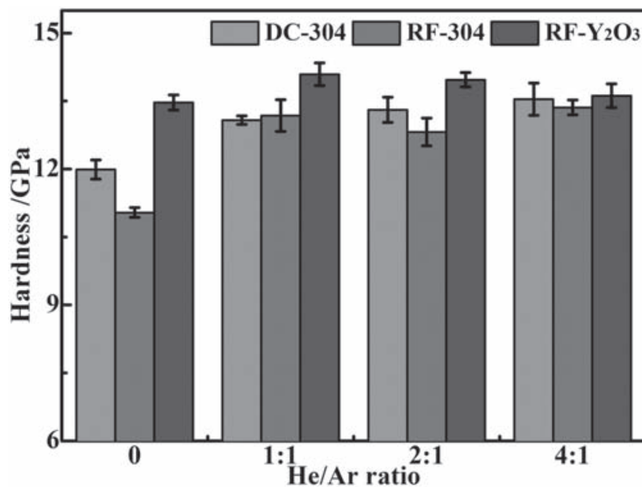

Figure 10. Nanoindentation hardness of the FeCrNi-based films versus He/Ar ratio at three different conditions of DC sputtering 304 stainless steel, RF sputtering 304 stainless steel and the composite target.

FeCrNi films, obvious hardening phenomena were observed. Further compared with the Y_2O_3-doped results, the hardness value of the Y_2O_3-doped FeCrNi films fabricated through RF magnetron sputtering is more stable and larger than that of undoped FeCrNi films, indicating that the addition of dispersion Y_2O_3 particles could enhance the hardness of the films and improve the stability of the mechanical properties. Considering hardening mechanisms, the nanoindentation results demonstrated that although both He atoms and Y_2O_3 particles can play an important role in improving the mechanical properties of the FeCrNi film, the hardening effects induced by Y_2O_3 particles are more predominant, as confirmed by the higher hardness value under the same He/Ar sputtering conditions. It is worth pointing out that to clearly understand the hardening mechanisms induced by He and nano-size Y_2O_3 particles, more investigations from the atomic scale would be necessary based on the combination of theoretical simulation and experimental studies.

4. Conclusion

He-charged ODS-FeCrNi films were deposited by RF plasma magnetron sputtering under a He and Ar mixed atmosphere at 150 °C, and He-charged FeCrNi films were also fabricated under the same conditions through DC/RF magnetron sputtering for comparison. The concentration of He was controlled by adjusting the He/Ar ratios to 0, 1:1, 2:1 and 4:1, respectively. AES-ICP and XPS analysis confirmed that the Y element exists as Y_2O_3 in the films and the content of Y_2O_3 is about 1.7%–2.1%. The cross-sectional SEM images confirmed that the obtained films are composed of dense columnar nanocrystals, which are finer and more uniform in RF-sputtered films. The He/Ar ratio has a great influence on the thickness of the films regardless of whether the mode of magnetron sputtering is DC or RF. Nanoindentation results showed that the hardness of the Y_2O_3-doped films has a higher value and better stability than that of the FeCrNi films fabricated through DC/RF magnetron sputtering 304 stainless steel, which have similar hardness values at each He/Ar ratio. ERD analysis shows that the FeCrNi films fabricated through DC/RF magnetron sputtering 304-stainless steel contain similar amount (~17 at.%) of helium. However, the amount of He in the DC-sputtered film changes little with the increasing depth, while it decreases from ~20 at.% around the surface to ~14 at.% at the depth of 140 nm in the RF-sputtered film. Much less He was detected in the Y_2O_3-doped FeCrNi films than in the films undoped with Y_2O_3 owing to the lower backscattering possibility of He on Y_2O_3 than on 304 stainless steel, as well as the inhibition effect of nano-sized Y_2O_3 particles on He.

Acknowledgments

This work was financially supported by National Natural Science Foundation of China (No. 11374299).

References

[1] Zinkle S J and Ghoniem N M 2000 *Fusion Eng. Des.* **51–52** 55
[2] Lee E H and Mansur L K 2000 *J. Nucl. Mater.* **278** 11
[3] Azevedo C R F 2011 *Engin. Fail. Anal.* **18** 1921
[4] Gaganidze E and Aktaa J 2013 *Fusion Eng. Des.* **88** 118
[5] Zinkle S J, Maziasz P J and Stoller R E 1993 *J. Nucl. Mater.* **206** 266
[6] Ghoniem M and Takata M L 1982 *J. Nucl. Mater.* **105** 276
[7] Gilbert M R *et al* 2013 *J. Nucl. Mater.* **442** S755
[8] Peng L *et al* 2011 *Fusion Eng. Des.* **86** 2624

[9] Weaver H T and Camp W J 1975 *Phys. Rev.* B **12** 3054
[10] Henry J *et al* 2009 *J. Nucl. Mater.* **386–388** 345
[11] Klueh R L *et al* 2002 *J. Nucl. Mater.* **307–311** 773
[12] Schaeublin R *et al* 2002 *J. Nucl. Mater.* **307–311** 778
[13] Edmondson P D *et al* 2011 *Scr. Mater.* **65** 731
[14] Lu C Y *et al* 2014 *J. Nucl. Mater.* **455** 366
[15] Chen S *et al* 2014 *J. Nucl. Mater.* **455** 301
[16] Mattox D M and Kominiak G J 1971 *Vac. Sci. Technol.* **8** 194
[17] Liu C Z *et al* 2007 *J. Phys. D: Appl. Phys.* **40** 2150
[18] Jia J P *et al* 2007 *Nucl. Instrum. Methods* B **263** 446
[19] Shi L Q *et al* 2005 *Thin Solid Films* **479** 52
[20] Liu C Z *et al* 2007 *Chin. Phys. Lett.* **24** 2357
[21] Picraus S T 1981 *Nucl. Instrum. Methods* **182–183** 413
[22] Krauss A R and Gruen D M 1976 *J. Nucl. Mater.* **63** 380
[23] Song L *et al* 2015 *Thin Solid Films* **589** 627
[24] SRIM website: http://srim.org
[25] Schiettekatte F *et al* 2004 *Nucl. Instrum. Methods Phys. Res.* B **219–220** 125
[26] Pharr G M, Herbert E G and Gao Y 2010 *Ann. Revi. Mater. Res.* **40** 271
[27] Pharr G M, Strader J H and Oliver W C 2009 *J. Mater. Res.* **24** 653